Water Condensation in gas distribution plates of PEMFCs: flow and removal from the grooved patterns of the plates
Proceedings of European Congress of Chemical Engineering (ECCE-6)
Copenhagen, 16-20 September 2007

Water condensation in gas distribution plates of PEMFCs: flow and removal from the grooved patterns of the plates

C. Bonnet,[a] J. Ramousse,[b] N. Doss,[a] F. Lapicque,[a] M. Boillot,[a]

[a]*Laboratoire des Sciences du Génie Chimique, CNRS-ENSIC, 1 rue Grandville, BP 20451, F- 54001 Nancy, France*
[b]*Institut de Recherche sur l'Hydrogène, Université du Québec à Trois-Rivières, 3351, boul. des Forges, C.P. 500, Trois-Rivières (QC) G9A 5H7, Canada*

Abstract

The effect of the gas dynamics on the flow of water droplets in two different designs of bipolar plates was studied. With the serpentine design consisting of five parallel channels, liquid water is formed at the inlet of the channels and flows faster in the lower channel of the five channels. These experimental observations have been confirmed by modelling of flow phenomena and heat transfer in the plate. Water-clogging in the channels and its accumulation in the collecting segments at the pattern edges were also observed. With the column-flow pattern, liquid droplets are efficiently removed under the gas pressure and gravity. Channeling of the liquid water was observed and the gas flow rate has no influence on the channeling location.

Keywords: PEMFC, water condensation, bipolar plate channels, modelling

1. Introduction

Bipolar plates represent key components of polymer electrolyte membrane fuel cells (PEMFC) because of their multiple functions. These plates allow distribution of fuel and oxidant to reactive sites of the electrode, collection of the produced current, and provide mechanical support for the cell. In addition they facilitate the removal of water produced from the reaction, and contribute to heat removal from the membrane electrode assembly (MEA).
Since one of the important functions of the bipolar - or flow - plate is to feed reactive gases to the electrodes, the performance of a PEMFC is strongly dependent on the transport processing occurring within the flow pattern. The geometry of bipolar plates has a significant effect on the flow phenomena and on the intensity of heat and mass transfer: it has therefore a large impact on the performance of the fuel cell.
Previous researchers as Cho et al. (2004), have shown the influence of the bipolar plate material or, as Scholta et al. (2006a), that of the channel geometries on PEMFC

electrical performance. According to Scholta et al. (2006b) the flow field pattern of bipolar plates is also to exert a significant effect on the water management. Water is necessary in PEMFC for sufficient proton conduction in the membrane. Water produced in the fuel cell can be partly in the form of liquid for high hydration of the inlet gases and high current densities. Presence of liquid water in too a significant amount can result in water-clogging in the grooved channels of the bipolar plates, also in the structure of the diffusion layer (Palan and Shepard (2006)), as well as in the catalyst layers (He et al. (2007)). For such conditions the activity of some parts of the fuel cell reduces, with possible instability of the voltage. It is well known that temperature, flow rates and hydration have to be carefully chosen for efficient operation at the nominal current.
Little is known on the effect of the gas dynamics on the mobility of the water droplets in the fuel cell channels (Golpaygan et al. (2005)). The present investigation was aimed at observing the flow of liquid water in the grooved structures of the bipolar plate in emulation experiments since Ramousse et al. (2007) showed that the condensation of the water occurs preferentially at the ribs of the bipolar plate channels according to non isothermal transport model. Emulation experiments were carried out using an inert cell consisting only of a bipolar plate covered by a Perspex polymeric plate, allowing visual observations using a high-speed camera: warm humidified air was fed to the half inert cell and vapour water condenses in the plate due to water cooling at the back of the plate. Two graphite 25 cm^2 plates with different flow pattern were used here. Air flow rate and its hydration were adjusted as representative operating conditions of actual FC tests. For the serpentine design, experimental results are confirmed by numerical simulations of temperature and velocities along the channels.

2. Experimental section and methods

2.1. Experimental set-up

Two different designs of graphite Electrochem plates with a geometric area of 5x5 cm^2 were studied (Figure 1): (a) the so-called serpentine design actually consisted in the series of seven sets of five parallel channels 47.7 mm long and 0.77 mm wide, with collecting and redistribution segments at the edge of the 5x5 cm^2, (b) in the column-flow, the gas was distributed through thirteen squared orifices, then circulated around 2x2x2 mm^3 tiles placed regularly on the plate surface, before being collected by the outlet tube.

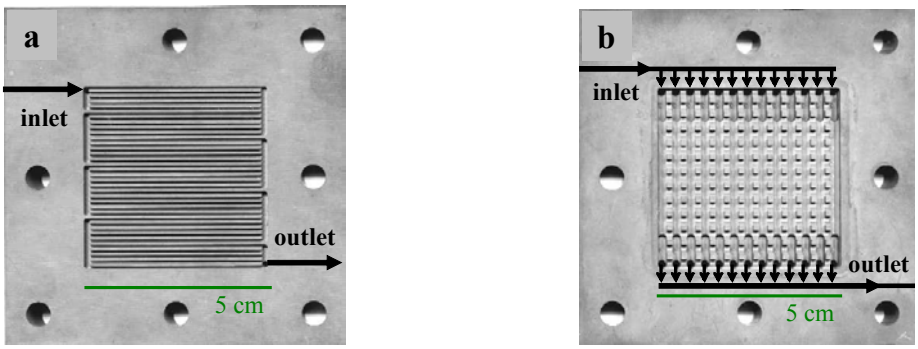

Figure 1 : Designs of graphite Electrochem plates.

A schematic diagram of the test bench is given in Figure 2. Before entering the half inert cell, air was precisely controlled by a flowmeter and was humidified in laboratory-designed packed columns filled with deionized water. The humidification temperature was fixed by control of the dew point of the packed bed columns, which were heated by an external water bath. The saturated air leaving the humidifier was fed to the emulation half-cell: water condensation in the inlet pipes was avoided by using wrapped heating wires and efficient thermal insulation. Tests revealed that the water content in the inlet gas corresponds to perfect saturation at the humidifier at the selected temperature.

The rear face of this plate was cooled by tap water at 18 °C for condensation of water vapour in the grooved distribution channels. A Perspex polymeric plate placed at the bipolar plate front allows to visualize the two phase flow. A silicone grease between the two plates allows water and gas leaks to be avoided. Systran high-speed video camera with up to 256x256 resolution and up to 1000 frames per second allowed continuous observation of the two-phase flow. At the outlet of the gas distribution channel, condensed water was collected. In the modelling of the gas temperature part, it was checked that the air released was saturated at the cooling water temperature. The bipolar plate was carefully dried at the end of each experiment.

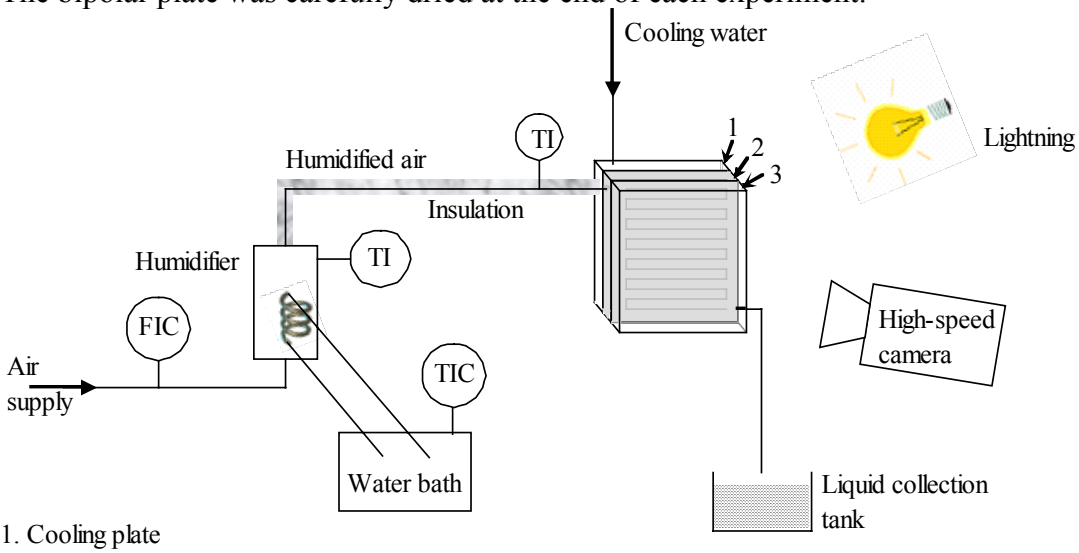

1. Cooling plate
2. Bipolar plate
3. Perspex polymeric plate

Figure 2 : Schematic diagram of the test bench.

2.2. Operating conditions

The volume flow rate of air injected into the emulation cell as its hydration had to be determined to correspond to operating conditions of the fuel cells used in previous investigations (Boillot (2005)). Only the air compartment of the FC was considered here since visualisation experiments were carried out with half the fuel cell. Oxygen is reduced at the cathode as follows:

$$O_2 + 4\,e^- + 4\,H^+ \rightarrow 2\,H_2O \quad (1)$$

The mole flow of oxygen consumed in the fuel cell for the production of current I is written as:

$$N_{O2}^{cons} = I/4F \quad (2)$$

where F is Faraday's constant. In fact the cathode is fed with air, with mole fraction of oxygen y_{O2}. In addition, reactant gases are always fed in excess in comparison with the flow rate actually consumed at the cathode. The flow rate of air injected is then expressed as:

$$N_{air}^{in} = \frac{I}{4F}\frac{\lambda_{O2}}{y_{O2}} \quad (3)$$

where λ_{O2} is the stoichiometric factor, term (λ_{O2}-1) corresponding to the excess. Experimental simulation was conducted for λ_{O2}=3 and for I = 1 and 3 A: corresponding volume flow rates of air injected are 50 and 150 STP cm^3 min^{-1}, respectively.

The flow rates calculated above are for dry gases. In fact, air is hydrated in a dedicated humidifier, whose design allows perfect saturation of the gas with water at the selected temperature, T_{sat}. The humidification temperature T_{sat} is chosen below the fuel temperature T_{FC} in order to control the relative humidity of the inlet gas, RH_{in}. The water flow in the humidified air at the inlet is thus given by:

$$N_{H2O,air}^{in} = \frac{y_{sat}(T_{FC})RH_{in}}{1 - y_{sat}(T_{FC})RH_{in}} N_{air}^{in} \quad (4)$$

Similar calculation could be made for hydrogen, with the appropriate value for the saturation temperature in the anode side. Besides water is produced by oxygen reduction and according to stoichiometric coefficients of the reduction, Faraday's law can be written as:

$$N_{H2O}^{prod} = I/2F \quad (5)$$

The total mole amount of water in the cell is then equal to:

$$N_{H2O}^{out} = N_{H2O,air}^{in} + N_{H2O,H2}^{in} + N_{H2O}^{prod} \quad (6)$$

For the considered emulation, only one compartment is considered, without current production, however the water flow rate has to be in accordance with real FC operations. The mole flow rate of water fed to the visualisation operation was then assumed to equal to the sum:

$$N_{H2O}^{vis} = N_{H2O,air}^{in} + N_{H2O}^{prod} \quad (7)$$

Calculations have been made for $T_{FC} = 75$ °C corresponding to $y_{sat}(T_{FC}) = 0.38$, $RH_{in} = 80$ %, leading to $T_{sat} = 70$ °C: for the current values of interest, the mole flow rate of water to be fed is respectively at 1.6 10^{-5} and 4.9 10^{-5} mole s^{-1} (i.e. 1.0 and 3.1 g h^{-1}).
The temperature of the humidifier for emulation experiments can be deduced from the mole flow rate of dry air, N_{air}^{in}, and the amount of water to be fed, N_{H2O}^{vis}, taking into account Rankine's law: this temperature found to be near 75 °C, was selected for the present investigations.

3. Modelling of the gas cooling and water condensation

A mathematical model has been developed in order to simulate the cooling of the saturated air in the feeding channels of the above visualization cell by the cooling of tap water behind the bipolar plate. This was done in view to predicting the temperature profile in the grooved pattern of the plate and the extent of water condensation. Only the serpentine-pattern was considered here. The model equations derive from heat and mass balances in element dx of the channel, as shown in Figure 3.

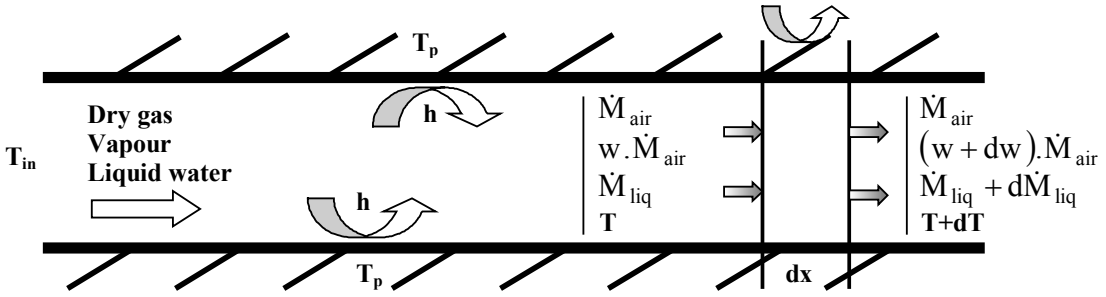

Figure 3: Parameters and variables of the model for gas cooling and condensation.

At the inlet, air is assumed saturated with water at the temperature T_{in}, corresponding to T_{sat} in the experiments. The wall temperature T_p was considered constant and set to 18 °C. The mass flow rate of dry gas, $\dot{M}_{air}$, was also constant - no air consumption in visualization cell. The water vapour flow was defined by the absolute humidity, w, and the dry gas flow rate. The water mass balance leads to the expression of liquid water production in element dx:

$$d\dot{M}_{liq} = -\dot{M}_{air}\, dw \quad (8)$$

Air was assumed saturated all along the channel at temperature T(x). Using Rankine's equation $\left(\ln(P_{sat}(T)) = 11.67 - \frac{3816.44}{T - 46.13} = a - \frac{b}{T - c} \right)$ and after linearization of the differential balances, the variation of the absolute humidity with gas temperature T could be expressed as follows:

$$dw = \frac{M_{eau}}{M_{air}} \frac{b}{(T-c)^2} \frac{1}{1-\exp\left(-a+\frac{b}{T-c}\right)} dT \quad \text{with a, b and c from Rankine's law (9)}$$

Finally, the enthalpy balance in the channel element with convective heat exchange at the walls, after simplification, leads to:

$$h.p.dx.(T-T_p) + \dot{M}_{air}.Cp_{air}.dT + w.\dot{M}_{air}.Cp_{vap}.dT + dw.\dot{M}_{air}.Cp_{vap}.T + dw.\dot{M}_{air}.\Delta H_{vap} + \dot{M}_{liq}.Cp_{liq}.dT + d\dot{M}_{liq}.Cp_{liq}.T = 0 \quad (10)$$

Where h is the heat transfer coefficient at the cooled wall. The three linearized equations (8), (9) and (10) were solved numerically for calculation of the temperature profile. The physical parameters used are given in Table 1:

	Air	*Vapour*	*Liquid water*
Cp (J g^{-1} K^{-1})	1.006	1.908	4.188
k (W m^{-1} K^{-1})	0.033	0.018	0.67
ΔH_{vap} (J g^{-1})			2389.7

Table 1: Physical properties of the fluids.

Heat transfer coefficient h was evaluated considering that the flow was steady laminar in the squared microchannel and assuming uniform wall temperature T_p:

$$Nu = \frac{hD_h}{k} = 2.98 \quad (11)$$

For dry air flowing in a 0.77 mm square channel coefficient h is equal to h = 128 W m^{-2} K^{-1}. The significant hydration of air has a low impact on the heat transfer coefficient because vapour and air have comparable thermal conductivities. However, the actual value for h is to be greater than the above estimate because of the presence of liquid water, with far higher thermal conductivity (Table 1). Heat transfer rates are likely underestimated and the air-vapour mixture is likely cooled more rapidly than predicted by the above model.

The model was worked for a humidification temperature of 75 °C and for flow rates of dry air of 50 and 150 STP cm^3 min^{-1}. The calculated temperature profiles along the channel length are reported in Figure 4:

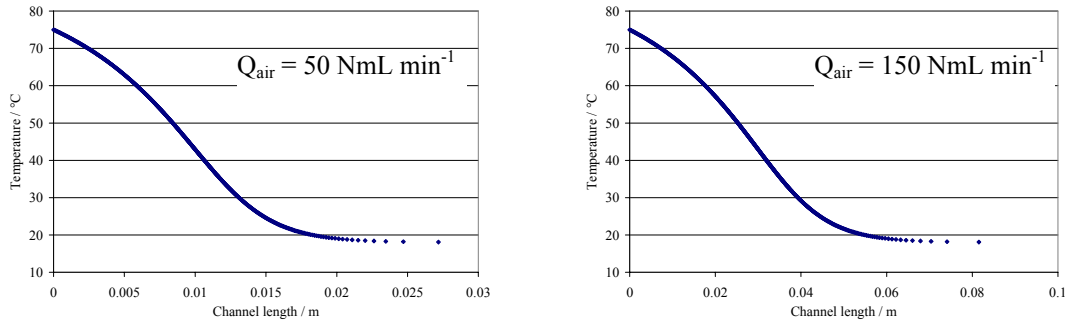

Figure 4: Temperature profile in the channel for dry air flow rates at 50 and 150 STP cm^3 min^{-1}.

The temperature of the gas was shown to decrease rapidly, and reached the wall temperature within 0.1 °C after 2.5 and 8 cm respectively for the two flow rates considered. Hence water condenses near the inlet of the channel, in particular for the lower air flow rate. In addition it has to be mentioned that in the real plate the gas does not enter directly in the gas distribution channel but 2 cm upstream of this channel. Therefore it can be considered that the gas temperature is uniform in a large part of the grooved pattern, and water is condensed in the first centimetres of any of the five 35 cm-long serpentine. Furthermore for the modelling of the gas velocity in the channels presented in the following section, air could be assumed at the cooling temperature as soon as it enters in the five parallel channels.

4. Modelling gas flow in the channel flow pattern

Most works on modelling of the flow phenomena by solving Navier-Stokes equations is carried out under assumption of incompressible flow of the Newtonian fluid. The incompressible flow assumption typically holds well for the cases of compressible fluid, such as air at room temperature and pressure. Taking into account the incompressible flow assumption and assuming constant viscosity and density, the Navier-Stokes equation is:

$$\frac{\partial u}{\partial t} + u \cdot \nabla u = g - \frac{1}{\rho}\nabla P + \frac{\mu}{\rho}\nabla^2 u \qquad (12)$$

Equation (12) has to be solved together with the continuity equation:

$$\nabla . u = 0 \qquad (13)$$

where u, t, g, ρ, μ and P represent the velocity, time, gravity, density, dynamic viscosity and pressure respectively. Equation (13) can be used since the temperature effect is neglected.

The motion of air in the serpentine design was modeled in 2-D by solving equations (12) and (13) with Femlab®. The flow rate of dry air was fixed at 50 STP cm^3 min^{-1}. Constant viscosity and density were taken at 18.5 10^{-6} Pa s and 1.2 kg m^{-3} respectively, and the bipolar plate was assumed isothermal at 18 °C from the calculations presented above.

Steady state was assumed and integration was performed subject to the following boundary conditions:

- at the inlet, the velocity profile is flat and was calculated straightforward from the considered flowrate,
- at the outlet, the relative pressure is equal to zero,
- at the walls, the gas velocity is zero, corresponding to zero slip velocity.

The modelling of the gas velocity in the serpentine design is shown in Figure 5:

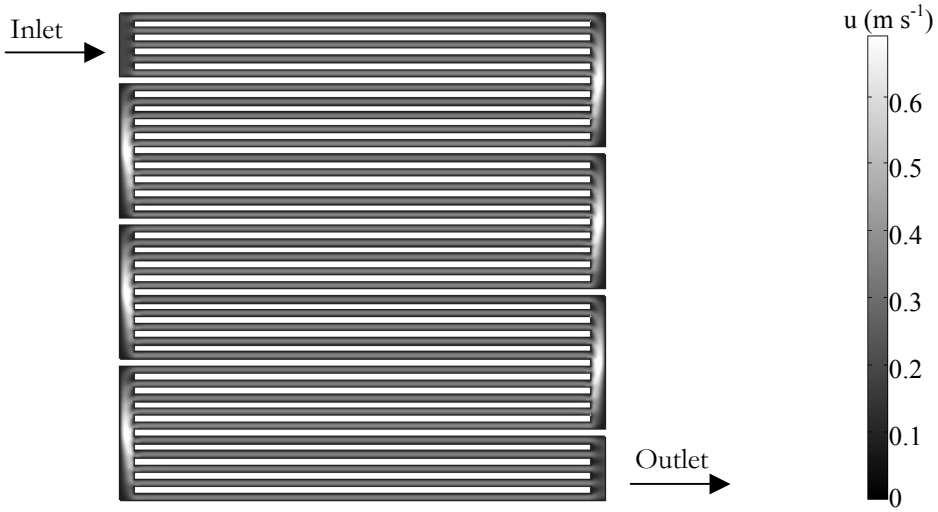

Figure 5: Gas velocity profile in the serpentine flow pattern (flow rate = 50 STP cm^3 min^{-1}).

The bipolar plate with serpentine flow pattern design used for the above modelling does not correspond exactly to the actual plate: as a matter of fact the vertical channels for collection and distribution of the gas, are narrower but deeper. A depth difference exists between the five parallel channels and the side collection/distribution channels. On top of that, for the model, the gas is assumed to enter on the overall length of the channel at the top left of the plate, and to exit on the overall length of the channel at the bottom right.

At each side volume, the model calculations revealed the presence of zones with very high velocity as corresponding to the local mixing of the fluid flowing in the five parallel channels. Zones with very sluggish flow appear on the very upper and lower parts of the side channels. In one channel the velocity remains constant all along the channel length. In the highest channel the velocity profile in the transverse direction is presented in Figure 6a: the obtained parabolic profile is typical of a laminar flow, which is in agreement with theory since viscous forces are far larger than inertia forces in microscale systems.

Velocity values slightly differ from one channel to another. Figure 6b presents the velocity values at the half-width of the five parallel channels. In each series of five parallel channels, the velocity is the slowest in the first higher channel (Channel 1 in Figure 6b), the highest in the fifth lower channel (Channel 5).

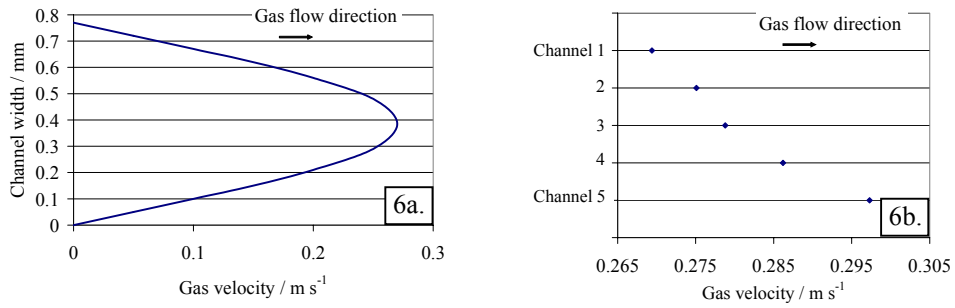

Figure 6: 6a. Velocity profile in the channel width. 6b. Value for the average velocity in the five parallel channels.

5. Experimental results

5.1. Serpentine pattern

Observations were made in the serpentine flow pattern with dry air at 50 STP cm^3 min^{-1} humidified at 75°C ($P_{sat}^{H20}(75°C) = 0.38$ atm).

Figure 7 illustrates the two-phase flow observed experimentally. The light regions in the picture correspond to the presence of water in the liquid form after condensation in the distribution channel of water vapour contained in the gas flow. Liquid water is formed as soon as it enters in the distribution channels of the bipolar plate. This result confirms the modelling of the gas temperature presented before. The liquid water front moves in the flow direction. The liquid water flows faster in the last fifth channel than in the first one. This result is in agreement with the model results presented in Figure 6b.

Figure 7: Liquid water in the serpentine design. Zoom in the upper part.

Although not perfectly clear in the picture, droplets of water are attached at low-shear areas in the side volume of the plate. This accumulation of liquid could be favoured by the negligible velocity calculated in the edge of the lateral part as shown in Figure 5. This accumulation could also explain that the last fifth channel is favoured for the transport of liquid water. Another phenomenon observed is the slug flow regime prevailing in the serpentine pattern. The presence of liquid water in the lateral part of the plate certainly reduces the gas access to the distribution channels. These droplets of water are suddenly removed by a slight overpressure of the gas and they flow rapidly in the channels. Figure 8 presents the fast draining of water since liquid water runs around 5 cm inside the channels within one second. The irregular transport phenomenon in such flow plates leads to lower performance of PEMFC as observed experimentally with serpentine plates operated at high current with greatly hydrated gases (Doss (2007)).

Figure 8: Fast draining of water in the serpentine pattern: the two pictures were taken at one-second interval.

Xu (1999) and Triplett et al. (1999) conducted experimental investigations for air/water two phase flow in microchannels. Different flow patterns, namely bubbly, churn, slug, annular patterns were identified depending on both water and air velocities. For the present investigation with narrow channels, the high-speed camera used did not allow the flow pattern in the channel to be distinguished. The recent acquisition of a faster camera (500 fps) would allow more precise observations, in particular for identification of the flow regime in the channels. Such identification is of great importance for modeling heat exchange between the flow and the channel walls.

5.2. Column flow pattern

As explained by Li and Sabir (2005) the column flow pattern results in low reactant pressure drop. However, reactants flowing through such flow patterns tend to follow the path of least resistance across the flow field, which is to lead to channeling and the formation of stagnant areas. It can therefore be expected uneven distributions of reactant, inefficient removal of produced water and poor fuel cell performance in particular regions of the cell. Boillot (2005) confirms these results by simulation of flow phenomena in this flow pattern: the flow fields calculated showed the presence of stagnant areas in the top right corner (gas inlet on top left corner) and in the bottom left corner (outlet in bottom right corner) where transport by diffusion seems to be part of the overall transport rate.
The two-phase flow in the column flow pattern was visualized with dry air at 50 or 150 STP cm^3 min^{-1} passing through the hydration chamber at 75°C. Figure 9 presents liquid water in the column flow pattern after 1h10 experiments for the two flow rates investigated. In the plate of interest, the liquid droplets formed are more regularly removed under the combined pressure of the gas and gravity: droplets falling entrain liquid water in their fall, in sort of avalanche phenomenon. The photographs taken are in qualitative agreement with the observations of Li and Sabir (2005), who also evidenced channeling of liquid water. Once a drop falls in a vertical channel, neighbouring liquid water at the wall is to be captured by the falling liquid by capillarity. Stagnant liquid water can also be observed in the gas collection channel at the outlet of the cell. Because of the pressure drop for both gas and liquid, interfacial forces govern the flow of the liquid, for which preferential flow is likely due to higher local hydrophilicity of the graphite surface. Comparative analysis of the photographs taken for the two flow rates showed that the above preferential flow does not depend on the dry air flow since for the higher flow rate the last channels are not preferentially chosen.


a.
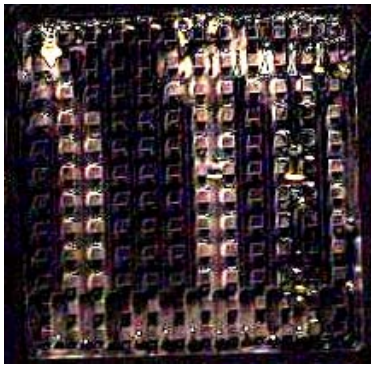
b.

Figure 9: Liquid water in the column-flow pattern with flowrate of dry air at 50 STP cm^3 min^{-1} (a), and 150 STP cm^3 min^{-1} (b).

6. Conclusion

The effects of the gas dynamics and of the bipolar plate design on the motion of the water droplets formed in a PEMFC were presented. A high-speed camera allowed to observe the condensation of water contained in humidified air driven to an emulation inert half cell. In the column-flow pattern, liquid water is regularly removed under the combined pressure of gas and gravity. Channeling of the liquid water appears independently of the gas flow rate. Stagnant liquid water was observed in the gas collection channel at the outlet of the cell. With the serpentine design consisting of five parallel channels, liquid water is formed at the inlet of the channels, as confirmed by preliminary calculations of temperature in the plate structure. It was also observed that liquid water flows faster in the lower channel of the five channels and the velocity decreases for upper channels. Modelling of gas flow is in agreement with this experimental observation. Besides, the serpentine pattern favours slug flow of liquid water in the channels. The liquid droplets present in the lateral part of the plate are suddenly removed by the slight overpressure created by transient gas accumulation, which renders transport phenomena irregular in such flow plates. This fact is perfectly consistent with the lower performance of PEMFC provided with serpentine plates operated at high current with greatly hydrated gases (Doss (2007)).

Reference

Boillot, M., (2005), (2005) *PhD Dissertation*, INPL, Nancy, France.
Cho, E.A., Jeon, U.-S., Ha, H.Y., Hong, S.-A., Oh, I.-H., (2004) *Journal of Power Sources,* 125, 178-182.
Doss, N., (2007) *Internal report LSGC*, INPL, Nancy, France.
Golpaygan, A., Ashgriz, N., (2005) *International Journal of Energy Research*, 29, 1027-1040.
He, G., Ming, P., Zhao, Z., (2007) *Journal of Power Sources,* 163, 864-873.
Li, X., Sabir, I., (2005) *International Journal of Hydrogen Energy*, 30, 359-371.
Palan, V., Shepard, W., (2006) *Journal of Power Sources,* 159, 1061-1070.
Ramousse, J., Didierjean, S., Lottin, O., Maillet, D., (2007) *Hydrogen and fuel cell 2007,* Vancouver, Canada.
Scholta, J., Häussler, F., Zhang, W., Küppers, L., Jörissen, L., Lehnert, W., (2006a) *Journal of Power Sources,* 155, 60-65.
Scholta, J., Escher, G., Zhang, W., Küppers, L., Jörissen, L., Lehnert, W., (2006b) *Journal of Power Sources,* 155, 66-71.
Triplett, K.A., Ghiaasiaan, S.M., Abdel-Khalik, S.I., Sadowski, D.L., (1999) *International Journal of Multiphase Flow*, 25, 377-394.
Xu, J., (1999) International Journal of Heat and Fluid flow, 20, 422-428.